Biol. Cybern. 69, 353–362 (1993)

Biological Cybernetics

Virtual trajectory and stiffness ellipse during multijoint arm movement predicted by neural inverse models

Masazumi Katayama [1], **Mitsuo Kawato** [2]

[1] Intelligent Systems Laboratory, Sanyo Electric Co., Ltd., Tsukuba Research Center, 2-1 Koyadai, Tsukuba, Ibaraki 305, Japan
[2] Department 3, ATR Human Information Processing Research Laboratories, 2-2 Hikaridai, Seika-cho, Soraku-gun, Kyoto 619-02, Japan

Received: 28 November 1992/Accepted in revised form: 5 March 1993

Abstract. We predict the virtual trajectories and stiffness ellipses during multijoint arm movements by computer simulations. A two-link manipulator with four single-joint muscles and two double-joint muscles is used as a model of the human arm. Physical parameters of the model are derived from several experimental data. Among them, special emphasis is put on low values of the dynamic hand stiffness recently measured during single-joint and multijoint movements. The feedback-error-learning scheme to acquire the inverse dynamics model and the inverse statics model is utilized for this prediction. The virtual trajectories are much more complex than the actual trajectories. This indicates that planning the virtual trajectory is as difficult as solving the inverse dynamics problem for medium and fast movements, and simply falsifies the advocated computational advantage of the virtual trajectory control hypothesis. Thus, we conclude that learning inverse models is essential even in the virtual trajectory control framework. Finally, we propose a new computational model to learn the complicated shape of the virtual trajectories by integrating the virtual trajectory control and the feedback-error-learning scheme.

1 Introduction

Voluntary arm movements are skillfully performed through both feedback and feedforward control mechanisms. Some feedforward control mechanisms appear indispensable, at least for relatively fast and well-coordinated multijoint movements. Control mechanisms employing only feedback cannot explain how deafferented monkeys can move their arms to a target without concurrent visual information (Polit and Bizzi 1979). The final position control hypothesis that specifies only the final target point (Bizzi et al. 1976) cannot describe how a monkey's arm perturbed while moving toward a target returns to an intermediate point on the intended trajectory (Bizzi et al. 1984).

Moreover, feedback control is limited by the transport delay associated with neural feedback loops and by the response delay included in sensory receptors and muscles: 30–100 ms for feedback through a somatosensory feedback loop, and 150–250 ms for visual feedback. Only slow movements can be executed stably by feedback control alone, because a large feedback gain gives rise to instability.

The fundamental question raised in this paper is how the central nervous system (CNS) executes feedforward control. Let us first briefly introduce previous hypotheses for posture control that make use of viscoelastic properties of the neural-musculoskeletal system. Rack and Westbury (1969) examined the length-tension curve of an individual muscle under isometric conditions and quantitatively ascertained that muscles exhibit spring-like behaviors. This muscle elasticity depends on the activation level of the muscle itself, and a higher muscle activation level results in greater stiffness. Fel'dman (1966) studied how the CNS makes use of such muscle properties and proposed an equilibrium point hypothesis: an equilibrium posture is determined as an intersection of the length-tension curves of agonist and antagonist muscles.

After extending the proposed mechanism for posture maintenance to movements, several research groups investigated a class of feedforward control mechanisms. The basic idea was to shift the equilibrium point continuously so that an intended movement is executed as a follow-up trajectory of the equilibrium-point motion. Hogan (1984) called the time series, defined as a succession of equilibrium points, a *virtual trajectory*. Consequently, a class of feedforward control schemes is often called virtual trajectory control, and sometimes equilibrium trajectory control.

In these schemes, the elastic muscle forces necessary for an intended trajectory are automatically generated as products of the difference between the virtual trajectory and the actual trajectory, and the muscle stiffness. The actual trajectory is therefore determined as a consequence of the interaction of the elastic muscle forces with

Correspondence to: M. Katayama

the dynamic forces (inertia, Coriolis forces, and so on). According to this hypothesis, the main role of the CNS is to preprogram the virtual trajectory. The advocated advantage is that the inverse dynamics problem is avoided.

Mussa-Ivaldi et al. (1985) measured and characterized the field of elastic forces associated with different hand postures in the horizontal plane. The measured stiffness ellipses were approximately oriented with the major axis pointing toward the shoulder, and the shape and orientation of the ellipses of a fixed posture were somewhat invariant for different subjects and different days, with only their size changing. Because hand paths are roughly straight regardless of the spatial anisotropy of the stiffness ellipses, the virtual trajectories must be dexterously planned. Flash (1987) simulated multijoint arm movements based on the virtual trajectory control hypothesis and concluded that the observed point-to-point hand trajectories, which are slightly curved, could be reproduced by using straight virtual trajectories based on the minimum-jerk criterion (Flash and Hogan 1985). Planning the straight virtual trajectories is obviously much easier than directly solving the inverse dynamics problem. Flash, however, assumed that the coefficients of the joint stiffness matrix during movements of 1 s duration were about one to four times larger than the static joint stiffness values at posture maintenance (Mussa-Ivaldi et al. 1985), and manually adjusted stiffness matrix coefficients so as to reproduce the actual arm movements.

The advocated advantage of the virtual trajectory control must be carefully examined based on measured values of dynamic stiffness during movements. If physical parameters such as inertia moments, masses, and lengths of links are given and the actual hand trajectory is fixed, the required joint torques are uniquely determined from the inverse dynamics equation. The human hand trajectories for point-to-point movements are roughly straight, with a bell-shaped tangential velocity profile (horizontal plane: Morasso 1981; Abend et al. 1982; Flash and Hogan 1985; Uno et al. 1989. vertical plane: Atkeson and Hollerbach 1985). Consequently, when the arm is in the high-stiffness state during movements, the virtual trajectory is close to the actual trajectory and could be very simple straight paths. On the other hand, if the dynamic stiffness values are rather small, the difference between the virtual and actual trajectories must become large to produce the required torques. In this case, the virtual trajectory has a very complicated shape, and for it to be planned might be very difficult. Thus, in the execution of fast and well-coordinated movements, the CNS must either increase the stiffness or preprogram a complicated shape of the virtual trajectory in order to compensate the dynamic forces and interaction forces between multiple links. To assess quantitatively the biological plausibility of the virtual trajectory control hypothesis, it is therefore essential to measure stiffness values during movements.

Dynamic stiffness values were recently measured by Bennett (1991), Bennett et al. (1992), and our group (Gomi et al. 1992). Based on these values, virtual trajectories and stiffness ellipses during multijoint arm movements were predicted by the *feedback-error-learning* scheme to acquire an inverse dynamics model and an inverse statics model for learning control of a dynamically redundant arm (Katayama and Kawato 1991a).

2 Virtual trajectory and dynamic stiffness during multijoint movement

2.1 Virtual trajectory

The dynamics equation for a multijoint arm in a horizontal plane can be generally written as

$$M(\theta)\ddot{\theta} + C(\theta, \dot{\theta})\dot{\theta} = \tau(\theta, \dot{\theta}, u) \tag{1a}$$

$$\tau(\theta, \dot{\theta}, u) = -A(\theta)^T T(l, \dot{l}, u) \tag{1b}$$

$$l = L(\theta) \tag{1c}$$

Here l and θ are the actual muscle length and joint angle vectors; $\dot{l} = \mathrm{d}l/\mathrm{d}t$; $\dot{\theta} = \mathrm{d}\theta/\mathrm{d}t$; $\ddot{\theta} = \mathrm{d}\theta^2/\mathrm{d}t^2$; $M(\theta)$ is the inertia matrix; $C(\theta, \dot{\theta})$ is the matrix that expresses the centrifugal, Coriolis, and friction forces; $\tau(\theta, \dot{\theta}, u)$ is the joint torque generated by agonist and antagonist muscles; $T(l, \dot{l}, u)$ is the muscle tension vector; $A(\theta)$ is the moment arm matrix that depends on the joint angle θ; superscript T denotes the transpose of a matrix; and u is the motor command vector fed to the muscles. The muscle lengths are uniquely determined from the joint angles, as described in (1c). The dimension of vectors θ and τ are equal to the number of joints n. The dimension of vectors u, T, and l are equal to the number of muscles m, and m is greater than n. The matrix $A(\theta)^T$ has the dimension $n \times m$.

When the motor command $u(t)$ is kept constant for an infinite time, the arm will eventually approach the equilibrium posture for that motor command value. This posture is a point at time t on a virtual trajectory. The equilibrium condition is derived from (1a) and (1b) as

$$0 = A[\theta_V(t)]^T T[l_V(t), 0, u(t)] \tag{2}$$

Here $\theta_V(t)$ and $l_V(t)$ are the virtual trajectories in joint-angle and muscle-length coordinates, respectively. The relation between $\theta_V(t)$ and $l_V(t)$ is given by (1c). The virtual trajectory $x_V(t)$ in hand coordinates is kinematically translated from the joint coordinates by a forward kinematics equation $X(\theta)$, as

$$x_V(t) = X[\theta_V(t)] \tag{3}$$

2.2 Dynamic stiffness

In this section, we define the dynamic stiffness during movement. The dynamics equation for a multijoint arm movement in the joint coordinates can be derived as follows:

$$\varphi(\theta, \dot{\theta}, \ddot{\theta}, u) = M(\theta)\ddot{\theta} + C(\theta, \dot{\theta})\dot{\theta} - \tau(\theta, \dot{\theta}, u) = 0 \tag{4}$$

In general, the restoring torque $\delta\varphi$ caused by small changes in the position $\delta\theta$, velocity $\delta\dot{\theta}$, acceleration $\delta\ddot{\theta}$, and the motor command δu can be described as

$$\delta\varphi = \frac{\partial\varphi}{\partial\ddot{\theta}}\delta\ddot{\theta} + \frac{\partial\varphi}{\partial\dot{\theta}}\delta\dot{\theta} + \frac{\partial\varphi}{\partial\theta}\delta\theta + \frac{\partial\varphi}{\partial u}\delta u \tag{5}$$

Let us assume here that the velocity, acceleration, and motor commands do not change during the perturbed movement when a small change $\delta\theta$ only in displacement occurs. According to this assumption, the dynamic joint stiffness R can therefore be defined as $\partial\varphi/\partial\theta$, and the restoring torque $\delta\varphi$ is derived as $(\partial\varphi/\partial\theta)\delta\theta$.

We introduce another possible definition of the dynamic joint stiffness which is more appropriate for examining the virtual trajectory control hypothesis. We define the joint stiffness as $\partial\tau/\partial\theta$ which is ascribed only to changes in muscle tensions caused by the positional displacement. This definition is more appropriate because the dynamic forces (e.g. inertia and Coriolis forces) act as external forces in the virtual trajectory control. We note that the new definition $(-\partial\tau/\partial\theta)$ of the stiffness is just a part of the above definition. Correspondingly, $\delta\varphi$ is calculated as $(-\partial\tau/\partial\theta)\delta\theta$. The restoring torques $\delta\varphi$ can be translated to the restoring hand force, δf, as

$$\delta f = (J^T)^{-1}\delta\varphi \tag{6}$$

Here, $J = \partial X/\partial\theta$ is the jacobian of $X(\theta)$, and $(J^T)^{-1}$ denotes the inverse of the jacobian transpose. The hand stiffness S is calculated from $\delta f/\delta x$ using small changes, δx, in the hand position.

3 A model of human arm and muscle

3.1 Muscle model

Muscles change their viscoelasticity depending on the nerve activation level. Here, we use a simple muscle model consisting of an elastic element and a viscous element arranged in parallel, since its parameters can be determined from previous studies. This model is called the Kelvin-Voight model (Özkaya and Nordin 1991). The muscle tension T is determined as

$$T(l, \dot{l}, u) = K(u)\{l_r(u) - l\} - B(u)\dot{l} \tag{7}$$

Here l is the muscle length vector and $\dot{l}$ is the contraction velocity vector. $K(u)$, $B(u)$, and $l_r(u)$ denote the muscle stiffness, the muscle viscosity, and the rest length of the muscle, respectively. In general, they depend on the motor command u, e.g., motoneuronal activations. We assume, however, for simplicity that $K(u)$, $B(u)$, and $l_r(u)$ are the following linear functions of the motor command u:

$$K(u) = k_0 + ku \tag{8a}$$

$$B(u) = b_0 + bu \tag{8b}$$

$$l_r(u) = l_0 + ru \tag{8c}$$

Here k and b are the elasticity and viscosity coefficients, respectively, and k_0 and b_0 are the intrinsic elasticity and viscosity. The term l_0 is the intrinsic rest length when u is zero, and r is a constant.

3.2 Two-link arm model with six muscles

It has been suggested that double-joint muscles play an important role in arm movement and force control

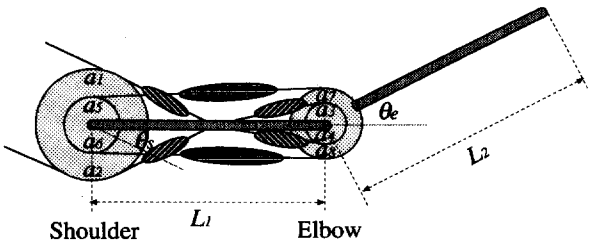

Fig. 1. Human arm model with four single-joint muscles and two double-joint muscles

(Hogan 1985; Tsuji et al. 1988; Flash and Mussa-Ivaldi, 1990). When only single-joint muscles were used in a human arm model, the shape of the stiffness ellipses became too narrow (Katayama and Kawato 1991b). In this paper, the human arm is modeled as a 2-link manipulator with four single-joint muscles and two double-joint muscles, as shown in Fig. 1.

By assuming constant moment arms that do not depend on joint angles, $A(\theta) = A$, the muscle length vector is given as

$$l = l_m - A\theta \tag{9}$$

$$A = \begin{pmatrix} a_1 & a_2 & 0 & 0 & a_5 & a_6 \\ 0 & 0 & a_3 & a_4 & a_7 & a_8 \end{pmatrix}^T \tag{10}$$

Here, (9) describes the detail by reducing (1c) with the above assumption. l_m is the muscle length when the joint angle θ is zero. The joint stiffness R and viscosity D are then derived as

$$R = \frac{\partial\tau}{\partial\theta} = A^T\frac{\partial T}{\partial l}\frac{\partial l}{\partial\theta} = A^T K(u) A \tag{11a}$$

$$D = -\frac{\partial\tau}{\partial\dot{\theta}} = A^T\frac{\partial T}{\partial\dot{l}}\frac{\partial\dot{l}}{\partial\dot{\theta}} = A^T B(u) A \tag{11b}$$

The joint stiffness and viscosity matrices here are symmetrical.

The dynamics equation of a planar 2-link arm is as follows:

$$\begin{pmatrix} I_1 + I_2 + M_2L_1^2 + 2M_2L_1L_{g2}\cos(\theta_e) & I_2 + M_2L_1L_{g2}\cos(\theta_e) \\ I_2 + M_2L_1L_{g2}\cos(\theta_e) & I_2 \end{pmatrix}\begin{pmatrix}\ddot{\theta}_s \\ \ddot{\theta}_e\end{pmatrix}$$
$$+ M_2L_1L_{g2}\sin(\theta_e)\begin{pmatrix} -2\dot{\theta}_e & -\dot{\theta}_e \\ \dot{\theta}_s & 0\end{pmatrix}\begin{pmatrix}\dot{\theta}_s \\ \dot{\theta}_e\end{pmatrix} = \begin{pmatrix}\tau_s \\ \tau_e\end{pmatrix} \tag{12}$$

Subscripts 1 and 2 indicate the upper arm and the forearm, respectively, and subscripts s and e indicate the shoulder joint and the elbow joint. The joint angle vector θ is $(\theta_s, \theta_e)^T$, I is the moment of inertia around the joint, L is the link length, L_g is the center of gravity of each link, and M is the link weight. The overall joint torque vector τ calculated from (1b) is $(\tau_s, \tau_e)^T$.

3.3 Arm parameters

The physical parameters of a two-link arm are estimated from previous measurements and summarized in Table 1. Morasso (1981) measured the lengths of the humerus and the forearm in adults and found that the difference between them ranged from 0 to 10 cm. In the present paper it is assumed that the upper arm is 30 cm long and the forearm is 35 cm long. The weights of the two links estimated in previous studies are used, and the moment of inertia around the joint is calculated from the length and weight of each link: $I_i = \frac{1}{3} M_i L_i^2$. The center of gravity for each link is determined according to Hatze's suggestions (Hatze 1979). Amis et al. (1979) examined the moment arm for each muscle around the elbow joint and found a nonlinear relationship between the moment arm and the joint angle. In this paper, however, we assumed constant-moment arms (Table 2) which correspond to the average values of anatomical data (Amis et al. 1979; Wood et al. 1989a, b).

3.4 Muscle parameters

Arm stiffness and viscosity are caused by the combined effects from muscle intrinsic properties and low-level neural reflexes. The complexity of the neural-musculoskeletal system makes it difficult to predict the joint or hand stiffness from the measured muscle stiffness *in vitro*. Elbow joint stiffness has been experimentally measured *in vivo* with small perturbations (Lacquaniti et al. 1982; MacKay et al. 1986) by using a linear second-order model of the motor apparatus. MacKay et al. found that the elbow stiffness values measured in different subjects ranged from 2 to 12 N·m/rad, the elbow viscosity values ranged from 0.1 to 0.2 N·m·s/rad, and the joint stiffness and viscosity depended on the joint angle. Mussa-Ivaldi et al. (1985) characterized the field of elastic forces as a stiffness ellipse. The measured hand-stiffness values ranged from about 100 to 450 N/m, and the elbow stiffness values estimated from the hand-stiffness values ranged from about 10 to 40 N·m/rad.

The measurements and analysis methods in previous studies were different, and the measured stiffness values therefore also differed considerably. The main reasons for the variations seem to be the coactivation of agonist and antagonist muscles, the difference between phasic and tonic properties in neural reflexes and muscle responses, the short-range stiffness (Joyce et al. 1969), and the tendon vibration (see Houk and Rymer 1981). The coactivation, the phasic properties, and the short-range stiffness induce higher stiffness values. For example, the stiffness increases as the amplitude of displacements decreases (Rack and Westbury 1969; MacKay et al. 1986).

The value of the dynamic stiffness could be very different from that of the static stiffness at posture maintenance, because, for example, the loop gains of neural reflexes may be suppressed by inhibitory descending signals from the CNS during movements. Bennett et al. (1992) measured the elbow joint mechanical impedance (stiffness, viscosity, and moment of inertia) during a single-joint cyclic movement at an amplitude of 1 rad with a period of 750 ms. In this experiment, small pseudorandom force disturbances were applied to the wrist with an airjet actuator. The mechanical impedance was estimated by an autoregressive moving average model (ARMA) using a quasilinear second-order model of the forearm. They found that the elbow stiffness values during cyclic movement were smaller than the rest stiffness at posture maintenance. In a related experiment, Bennett (1991) measured joint stiffness values during discrete elbow joint movement by using a powerful direct-drive motor to apply positional perturbations and then to measure the resulting torques. Although the two methods differed, the estimated dynamic stiffness values were similar. The measured dynamic stiffness and viscosity values changed somewhat independently (Bennett et al. 1992). The stiffness ranged from 2 to 9 N·m/rad, and the viscostiy ranged from 0 to 0.7 N·m·s/rad during movements.

The muscle stiffness and viscosity parameters shown in Table 3 were chosen so that the synthesized elbow stiffness and viscosity values matched the range of dynamic stiffness measured by Bennett (1991) and Bennett et al. (1992). For this choice, two simplifying assumptions were made. First, at the functional standard posture with the shoulder joint angle of 45° and the elbow joint angle of 70°, all motor commands were assumed to be zero. Thus, in our model, the muscle stiffness and viscosity values are minimal at the functional standard posture. Second, we assumed that all of the stiffness values of six muscles were identical as well as all of the viscosity values. Under this assumption, the ratio of shoulder to elbow stiffness measured by Flash and Mussa-Ivaldi (1990) around the functional standard posture could be reproduced. The joint stiffness and viscosity values at the functional standard posture were estimated as

$$R_{\text{standard}} = \begin{pmatrix} 3.9 & 1.6 \\ 1.6 & 3.0 \end{pmatrix} \text{N·m/rad}$$

$$D_{\text{standard}} = \begin{pmatrix} 0.26 & 0.11 \\ 0.11 & 0.20 \end{pmatrix} \text{N·m·s/rad}$$

Table 1. Arm parameters

	M (kg)	L (m)	L_g (m)	I (kg·m²)
Link 1	1.59	0.3	0.18	0.0477
Link 2	1.44	0.35	0.21	0.0588

M, link weight; L, link length; L_g, center of gravity of each link; I, moment of inertia around joint

Table 2. Moment arms

	a_1, a_2	a_3, a_4	a_5, a_6	a_7, a_8
Moment arm (cm)	4.0	2.5	2.8	3.5

a_1, shoulder flexor; a_2 shoulder extensor; a_3, elbow flexor; a_4, elbow extensor; a_5 and a_6, double-joint flexor; a_7 and a_8, double-joint extensor

Table 3. Muscle parameters

	k (N/m)	k_0 (N/m)	b (N·s/m)	b_0 (N·s/m)	r (cm)	$l_m - l_0$ (cm)
Shoulder flexor	1621.6	810.8	108.1	54.1	− 3.491	9.076
Shoulder extensor	1621.6	810.8	108.1	54.1	3.491	− 2.793
Elbow flexor	1621.6	810.8	108.1	54.1	− 2.182	5.672
Elbow extensor	1621.6	810.8	108.1	54.1	2.182	0.436
Two-joint flexor	1621.6	810.8	108.1	54.1	− 5.498	14.294
Two-joint extensor	1621.6	810.8	108.1	54.1	5.498	− 1.343

k and b are the elastic and viscosity coefficients, respectively; k_0 and b_0 are the intrinsic elasticity and viscosity; r, constant; l_0, intrinsic rest length. The values of r for single-joint muscles changes 50° in the joint angle when a motor command changes from 0 to 1. The change for double-joint muscles is 100°. The values of $l_m - l_0$ are chosen so as to reconstruct the defined functional standard posture with 0 motor commands

The value of the damping ratio of the forearm, defined as $D_{ee}/\sqrt{4I_2R_{ee}}$, was 0.24. The coefficient r was determined from the isometric length-tension curves measured by Rack and Westbury (1969). The values of $l_m - l_0$ were chosen so as to reproduce the defined functional standard posture. With these parameters, the damping ratio increased with increasing number of motor commands. The shoulder joint could move within the range of − 90 to 180°, and the elbow joint could move within the range of 0 to 180°.

4 Simulation results

We previously proposed a *parallel-hierarchical neural network* model that acquires an inverse statics model (ISM) and an inverse dynamics model (IDM) of the motor apparatus (Katayama and Kawato 1991a). The main role of the ISM is to achieve an intended posture, and that of the IDM is to compensate for the dynamic forces of the arm during fast movements. Two inverse models in combination can calculate the motor commands to achieve a desired movement trajectory. The human arm is a redundant controlled object at the dynamics level, that is, the number of muscles exceeds the number of joints. Acquisition of the inverse models is therefore an ill-posed problem in the sense that the motor commands cannot be determined uniquely from the desired trajectory. Because this redundancy problem is solved based on a *minimum-muscle-tension-change* criterion (Uno et al. 1989) in our neural network model (Katayama and Kawato 1991a), the values of the motor commands are approximately minimal and the coactivation level of agonist and antagonist muscles is also low. The virtual trajectory was calculated from (2) while inputting the motor commands calculated by the parallel inverse models.

4.1 Stiffness ellipses during posture maintenance

The ISM structured as a three-layer perceptron with 2-30-6 units was first trained during posture control. The orientation and shape of the predicted stiffness ellipses shown in Fig. 2 were similar to those measured by Mussa-Ivaldi et al. (1985). The shape narrowed as the hand approached the work-space boundary, and the stiffness ellipses were oriented with the major axis roughly pointing toward the shoulder. The major axis gradually turned toward the elbow as the hand approached the body. Note that the hand stiffness values measured by Mussa-Ivaldi were about six to ten times larger than those estimated by our simulation. This is because, as already explained, we estimated muscle stiffness parameters based on dynamic stiffness values measured by Bennett (1991) and Bennet et al. (1992).

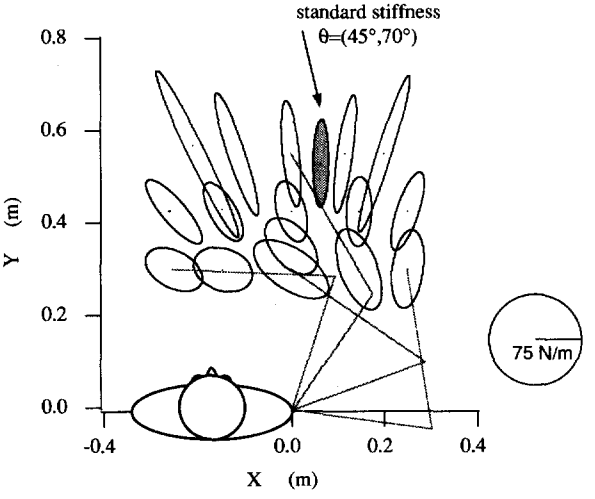

Fig. 2. Stiffness ellipses predicted at posture maintenance in a horizontal plane. The *shaded ellipse* is the stiffness ellipse at the functional standard posture where the shoulder angle is 45° and the elbow angle is 70°

4.2 Virtual trajectories and stiffness ellipses during movement

In order to evaluate the plausibility of the human arm model and the estimation method used in this paper, we first predicted the virtual trajectories in single-joint forearm movements. The shoulder joint angle was fixed, and two elbow-joint muscles and two double-joint muscles were used. The virtual trajectories were similar to those simulated by Hogan (1984) and were as simple as the desired or actual trajectories.

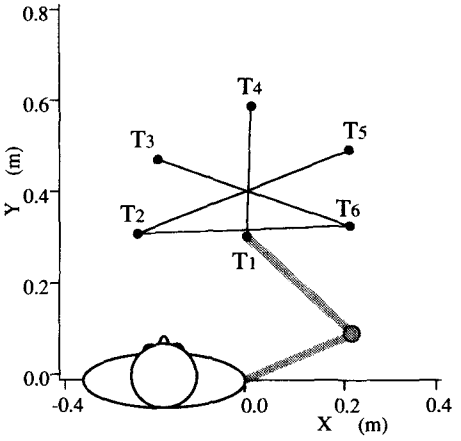

Fig. 3. Target positions for point-to-point movements in a horizontal plane at the shoulder level

The IDM was a three-layer perceptron with 6-30-6 neuron units. The IDM learning was performed while using the previously trained ISM. The desired trajectories were planned as the minimum-jerk trajectory (Flash and Hogan 1985). The target locations for four different movements T_2–T_6, T_2–T_5, T_3–T_6, and T_4–T_1 are shown in Fig. 3. IDM training was carried out for each movement with a duration of 750 ms. The stiffness ellipses during each movement were predicted (see Fig. 4) while using the motor commands calculated by the two trained inverse models (see Sect. 2.2). Note that the predicted stiffness values are not influenced by the terms M and C in (4), as mentioned in Section 2.2.

The orientation, size, and shape of the ellipses were quite different from those at posture maintenance (Katayama and Kawato 1992) because the IDM outputs are significantly large during movements. These characteristics strongly depended on the orientation, amplitude, and speed of the movement and the initial hand position. Although the dynamic hand stiffness matrices during movements are not generally symmetrical, the predicted ones were almost symmetrical. Matrix elements of hand stiffness S as functions of time are shown in Fig. 5.

The virtual trajectories were similarly predicted from (2) and (3). Figure 6 shows the desired, actual, and virtual trajectories for the four movements, and also shows the corresponding tangential velocity profiles. Because the IDM training was not perfect, there was a difference between the desired and actual trajectories. As can be seen, the predicted virtual trajectories were curved and were more complex than the actual trajectories. This is because of the lower dynamic stiffness, strong dynamic forces (inertia, Coriolis forces, and so on) associated with medium-speed movements, and spatial anisotropy of the stiffness ellipses. The minimum-jerk point-to-point trajectories had a bell-shaped tangential velocity profile, but some of the profiles of the virtual trajectories had two more peaks. For slower movements, the virtual trajectories were closer to the actual trajectories. For faster movements, however, the virtual trajectories were much more complex than the actual trajectories (Katayama and Kawato 1992). Moreover, Fig. 7 shows that the virtual trajectories represented in the joint coordinates were as complex as the virtual trajectories represented in the cartesian coordinates. These results indicate that it is not easy to plan the virtual trajectory either in task coordinates or in joint coordinates.

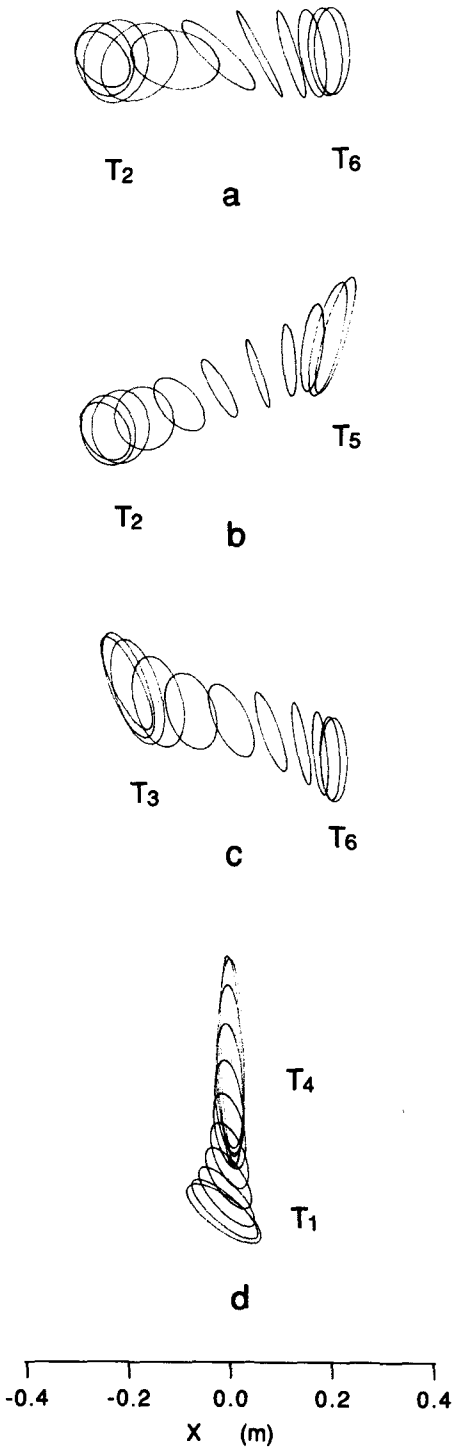

Fig. 4a–d. Stiffness ellipses predicted during 750-ms movements in a horizontal plane: **a** T_2–T_6; **b** T_2–T_5; **c** T_3–T_6; **d** T_4–T_1

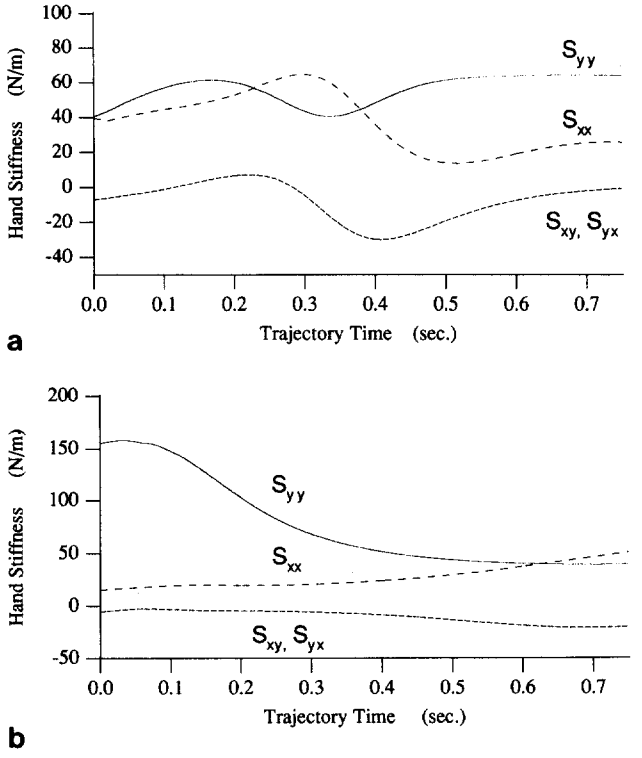

Fig. 5a, b. The elements of the hand stiffness matrix S during point-to-point movements of 750-ms duration in a horizontal plane **a** T_2–T_6; **b** T_4–T_1

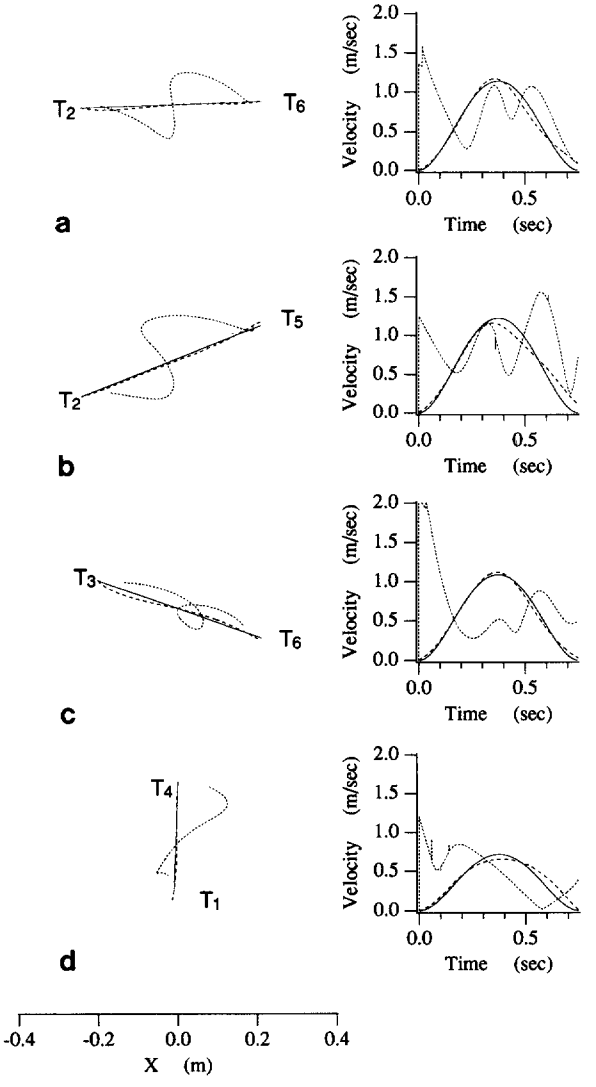

Fig. 6a–d. Virtual trajectories and tangential velocity profiles predicted during point-to-point movements of 750-ms duration in a horizontal plane. *Solid*, *dashed*, and *dotted lines* show the desired, actual, and virtual trajectories, respectively. **a** T_2–T_6; **b** T_2–T_5; **c** T_3–T_6; **d** T_4–T_1

The motor commands to six muscles during T_2–T_6 750-ms movement are shown in Fig. 8. Here, for the T_2–T_6 750-ms movement, the dynamic joint stiffness coefficients were less than 1.3 times the rest values. Specifically, the element R_{ss} ranged from 4.4 to 5.6 N·m/rad, R_{ee} ranged from 3.5 to 4.4 N·m/rad, R_{se} and R_{es} ranged from 1.7 to 2.3 N·m/rad, and the damping ratio of the forearm ranged from 0.26 to 0.29. The element S_{xx} of the dynamic hand stiffness ranged from 14 to 65 N/m, S_{yy} ranged from 40 to 64 N/m, and S_{xy} and S_{yx} ranged from −7 to 29 N/m. For the static hand stiffness at posture maintenance along the T_2–T_6 trajectory, S_{xx} ranged from 25 to 63 N/m, S_{yy} ranged from 35 to 71 N/m, and S_{xy} and S_{yx} ranged from −10 to 16 N/m. We found that some of the dynamic stiffness values were smaller than the rest stiffness at posture maintenance. This is because some of the motor commands, i.e., the sum of the ISM and IDM outputs, were smaller than the ISM outputs required to maintain the posture, as shown in Fig. 8.

In addition to the above simulations, we examined the virtual trajectories and the stiffness ellipses for two different sets of the stiffness and viscosity values (Katayama and Kawato 1992). Under one condition, the elbow stiffness value at the functional standard posture was 5.0 N·m/rad, which is the average of the maximum and minimum values during movements measured by Bennett et al. (1992). Under the other condition, the value was 16.8 N·m/rad, which is close to the value measured by Mussa-Ivaldi et al. (1985) at posture maintenance. For the former case, the predicted virtual trajectories were more complex than the desired trajectories, but were slightly simpler than the virtual trajectories shown in Fig. 6, because of slightly larger stiffness values. For the latter case, using considerably larger stiffness values, the predicted virtual trajectories became simpler, but the virtual trajectories for ballistic 250-ms movements were much more complex than the actual trajectories. In summary, by computer simulation we confirmed that the virtual trajectories become simpler as the dynamic stiffness values increase.

5 Discussion

Virtual trajectories and stiffness ellipses were predicted by learned inverse statics and dynamics models. The

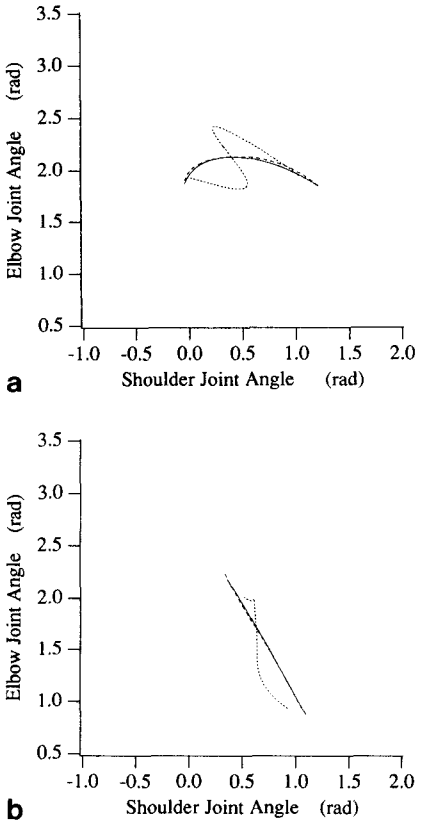

Fig. 7a, b. Virtual trajectories predicted in joint coordinates. *Solid*, *dashed*, and *dotted lines* show the desired, actual, and virtual trajectories, respectively. **a** 750-ms T_2–T_6 movement; **b** 750-ms T_4–T_1 movement

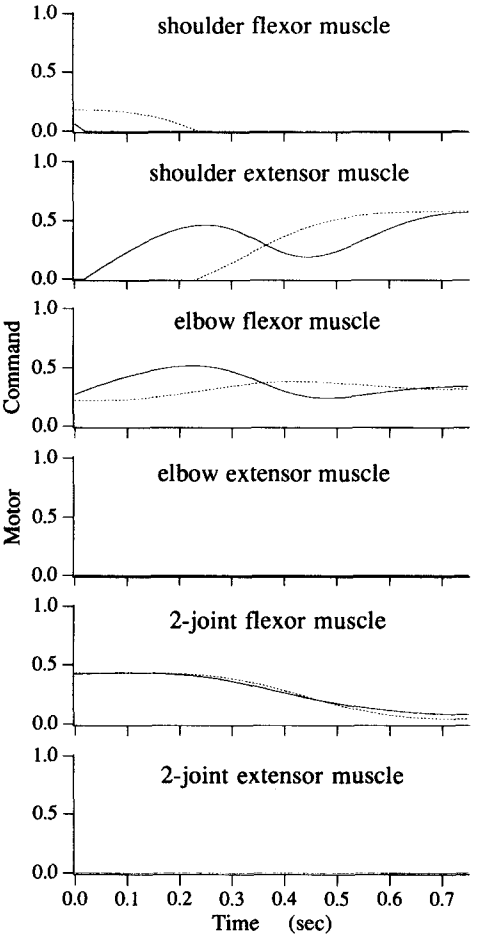

Fig. 8. Motor commands to six muscles during T_2–T_6 750-ms movement. *Solid curves*, Sum of the ISM and IDM outputs; *dotted curves*, ISM output

predicted virtual trajectories for medium-speed movements were curved, and much more complex than the actual trajectories. Thus, we found that planning the virtual trajectories is not easy and appears to be as complex as solving the inverse dynamics problem. However, we must note that this conclusion heavily depends on a couple of assumptions made in this study. First, as mentioned above, virtual trajectory profiles critically depend on the stiffness values during movement. But unequivocal estimation of them is technically difficult. Second, how to determine the motor commands is not at all apparent. The coactivation level of pairs of muscles in this simulation was low because instantaneous minimization of muscle-tension change was adopted in this study.

Flash's simulation results (1987) differed from ours even for relatively slow movements. The differences can be readily understood from the difference in assumed stiffness values. For T_2–T_6 movement, Flash (1987) assumed that R_{ss}, R_{se}, and R_{ee} of the dynamic joint stiffness matrix during 1-s movement are 80.7, 42.9, and 68.9 N · m/rad, respectively. On the other hand, based on experimental data, we assumed 5.1, 2.0, and 3.9 N · m/rad for the same movement with an even shorter duration of 750 ms. Our values were about 2.5–5% of those assumed by Flash (1987). Moreover, Flash (1987) assumed a wide range of the values of the damping ratios during movements: 0.35 to 1.5; the values of the damping ratios were larger than those used in our simulation. However, previous measurements indicated that the human arm is an underdamped system (Lacquaniti et al. 1982; MacKay et al. 1986; Bennett et al. 1992). The virtual trajectories predicted by using an arm model that roughly approximates a critically damped system were also more complex than the actual trajectories, although their profiles differed from those shown in Fig. 6 (Katayama and Kawato 1991b).

For posture control, the orientation and shape of the predicted stiffness ellipses were similar to those measured by Mussa-Ivaldi et al. (1985). For single-joint movement, however, the dynamic range of the simulated stiffness (i.e., 3.0 to 3.9 N · m/rad) was narrower than Bennett et al.'s experimental data (1992). This might be partly due to the difference between the point-to-point movements studied here and the cyclic movements studied by Bennett and colleagues. In their experiment, the coactivation of pairs of muscles may have occurred just before reaching targets during cyclic movement. On the other hand, the adopted instantaneous minimization of muscle-tension change did not produce any significant

coactivation. Although the minimum-muscle-tension-change criterion is effective from the standpoint of energy consumption in muscles, postures and movements may be more stably controlled when coactivation is effectively utilized. We need to examine further how to explain such a coactivation mechanism. One possible strategy would be to use a learning control model based on the *minimum-motor-command-change* model (Kawato 1992) rather than the minimum-muscle tension-chage model (Uno et al. 1989), because the feedback control law related to the minimum-motor-command-change model can explain the coactivation of a pair of muscles (Katayama and Kawato 1991a).

We have believed that the values of the dynamic stiffness are larger than these of the static stiffness. However, Bennett et al. (1992) found that the elbow stiffness values during cyclic movement are smaller than the values of the rest stiffness at posture maintenance. Moreover, Gomi et al. (1992) recently measured the time-varying stiffness of a multijoint arm during discrete point-to-point movements rather than single-joint movement and found that some of the dynamic stiffness values are smaller than the static stiffness at posture maintenance. The value of the hand stiffness component S_{yy} ranged from 50 to 200 N/m during T2–T6 750-ms movement. The simulation results presented in this paper, that some of the dynamic stiffness values are smaller than these of the static stiffness, may agree with the experimental findings by Bennett et al. (1992) and Gomi et al. (1992), and the range of the same component S_{yy} predicted in this simulation also agrees with the range in Gomi's experiments. Furthermore, the temporal waveform of the stiffness change is similar to the Gomi's data.

An alternative approach to the virtual trajectory control hypothesis is to solve directly the inverse dynamics and kinematics problems by using learned internal models of motor systems (for example, Kawato et al. 1987; Miller 1987; Atkeson and Reinkensmeyer 1988; Gomi and Kawato 1990; Katayama and Kawato 1991a; Jordan and Rumelhart, 1992). In general, it is computationally and mathematically difficult to acquire the inverse models for highly nonlinear and redundant controlled objects. However, we found that planning the complicated virtual trajectory is similarly difficult. We believe that the virtual trajectories for fast or medium-speed movements are quite complicated and are, thus, carefully planned beforehand.

However, the virtual trajectory control may be computationally effective for slow movements or under high stiffness conditions because the virtual trajectories could be quite simple in their shapes. We can summarize that when the human elbow stiffness values are less than about 15 N·m/rad, it is essential to solve the inverse dynamics problem or to plan the complicated virtual trajectories even for slow movements. In contrast, when the human elbow stiffness values are larger than about 15 N·m/rad, the virtual trajectory control may explain the feedforward arm control. Considering these, we finally propose an integrated computational scheme to acquire complicated shapes of virtual trajectories by motor learning.

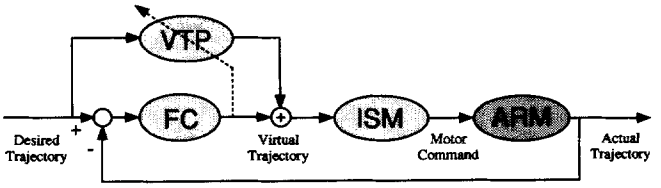

Fig. 9. A new computational scheme for learning control of arm movement which integrates the virtual trajectory control hypothesis and the feedback-error-learning scheme. *VTP* stands for the virtual trajectory planner, which calculates the necessary virtual trajectory while receiving the desired trajectory. *ISM* is the inverse statics model which transforms the virtual trajectory into the necessary motor commands which achieve the specified equilibrium posture. The arm is a controlled object. In parallel to the basic negative feedback loop, the VTP is overlaid as a feedforward controller, and in some sense as an inverse dynamics model of the downstream controlled object (cascade combination of the ISM and the arm). Because the input and the output of VTP are represented in the common coordinates, it does not need to address the coordinate transformation problem from the cartesian coordinates to the joint, muscle, or motor-command coordinates. While the ISM deals with the coordinate transformation problem, the VTP solves only the inverse dynamics problem

Figure 9 shows the architecture of the integrated model. The virtual trajectory planner (VTP) represents a model which calculates the virtual trajectory from the desired trajectory. The intended movement is performed by inputting the virtual trajectory calculated by the VTP into the inverse statics model. There are several advantages with this scheme. First, the VTP can be a unity function for slow movements or high stiffness conditions. Thus, the CNS can start to learn movements under slow movement conditions or high stiffness conditions, then adapt VTP to fast movements with low stiffness (known as a continuation method in engineering; see related work by Sanger 1992). Second, as the input and the output of the VTP are represented in the same coordinates, it is quite straightforward to design the feedback controller (FC in Fig. 9), which is the most difficult part of feedback-error learning. One of our future projects is to examine the computational efficiency and biological plausibility of this integrated scheme.

Acknowledgements. We are grateful to Drs. Masaaki Sato, Yasuhiro Wada, Menashe Dornay, Yasuharu Koike, Hiroaki Gomi, David Bennett, and Tery Sanger for their helpful comments and discussions during preparation of this manuscript. The main part of this work was done while the first author was at ATR Auditory and Visual Perception Research Laboratories. This work was supported by a Human Frontier Science Program Grant to M. Kawato.

References

Abend W, Bizzi E, Morasso P (1982) Human arm trajectory formation. Brain 105:331–348

Amis AA, Dowson D, Wright V (1979) Muscle strengths and musculoskeletal geometry of the upper limb. Eng Med 8(1):41–48

Atkeson CG, Hollerbach JM (1985) Kinematic features of unrestrained vertical arm movement. J Neurosci 5:2318–2330

Atkeson CG, Reinkensmeyer DJ (1988) Using associative content-addressable memories to control robots. In: Proceedings of the IEEE Conference on Decision and Control, pp 792–797

Bennett DJ (1991) Relationship between stiffness and net joint torque during ballistic elbow joint movement. Soc Neurosci Abstr 17:1029

Bennett DJ, Hollerbach JM, Xu Y, Hunter IW (1992) Time-varying stiffness of human elbow joint during cyclic voluntary movement. Exp Brain Res 88:433–442

Bizzi E, Polit A, Morasso P (1976) Mechanism underlying achievement of final head position. J Neurophysiol 39:435–444

Bizzi E, Accornero N, Chapple W, Hogan N (1984) Posture control and trajectory formation during arm movement. J Neurosci 4(11):2738–2744

Fel'dman AG (1966) Functional tuning of the nervous system with control of movement or maintenance of a steady posture. III. Mechanographic analysis of execution by man of the simplest motor tasks. Biophysics 11:766–775

Flash T (1987) The control of hand equilibrium trajectories in multi-joint arm movement. Biol Cybern 57:257–274

Flash T, Hogan N (1985) The coordination of arm movements: an experimentally confirmed mathematical model. J Neurosci 5(7):1688–1703

Flash T, Mussa-Ivaldi FA (1990) Human arm stiffness characteristics during the maintenance of posture. Exp Brain Res 82:315–326

Gomi H, Kawato M (1990) Learning control for a closed loop system using feedback-error-learning. In: Proceedings of the 29th IEEE Conference on Decision and Control, Hawaii, pp 3289–3294

Gomi H, Koike Y, Kawato M (1992) Human hand stiffness during discrete point-to-point multi-joint movement. Proc IEEE EMBS 1628–1629

Hatze H (1979) A model for the computational determination of parameter values of anthropomorphic segments. Technical report TWISK 79, National Research Institute for Mathematical Sciences, CSIR, South Africa

Hogan N (1984) An organizing principle for a class of voluntary movements. J Neurosci 4(11):2745–2754

Hogan N (1985) The mechanics of multi-joint posture and movement control. Biol Cybern 52:315–331

Houk JC, Rymer WZ (1981) Neural control of muscle length and tension. In: Brookhart JM, Mountcastle VB, Brooks VB, Geiger SR (eds) Handbook of physiology, vol 2. American Physiological Society, Bethesda, Md, pp 257–323

Jordan MI, Rumelhart MI (1992) Forward models: supervised learning with a distal teacher. Cognitive Sci 16:307–354

Joyce GC, Rack PMH, Westbury DR (1969) The mechanical properties of cat soleus muscle during controlled lengthening and shortening movements. J Physiol (Lond) 204:461–474

Katayama M, Kawato M (1991a) Learning trajectory and force control of an artificial muscle arm by parallel-hierarchical neural network model. In: Lippmann RP, Moody JE, Touretzky DS (eds) Advances in neural information processing systems, vol 3. Morgan Kaufmann, San Mateo, Calif, pp 436–442

Katayama M, Kawato M (1991b) Virtual trajectory and stiffness ellipse during force-trajectory control using a parallel-hierarchical neural network model. In: Fifth International Conference on Advanced Robotics, Pisa, Italy, pp 1187–1194

Katayama M, Kawato M (1992) Virtual trajectory and stiffness ellipse during multi-joint arm movement predicted by neural inverse models, ATR Technical Report TR-A-0144

Kawato M (1992) Optimization and learning in neural networks for formation and control of coordinated movement. In: Meyer D, Kornblum S (eds) Attention and performance, XIV: synergies in experimental psychology, artificial intelligence, and cognitive neuroscience – a silver jubilee. MIT Press, Cambridge, Mass, pp 821–849

Kawato M, Furukawa K, Suzuki R (1987) A hierarchical neural-network model for control and learning of voluntary movement. Biol Cybern 57:169–185

Lacquaniti F, Licata F, Soeching JF (1982) The mechanical behavior of the human forearm in response to transient perturbations. Biol Cybern 44:35–46

MacKay WA, Crammond DJ, Kwan HC, Murphy JT (1986) Measurements of human forearm viscoelasticity. J Biomech 19(3):231–238

Miller WT (1987) Sensor-based control of robotic manipulators using a general learning algorithm. IEEE J Robotics Automation 3:157–165

Morasso P (1981) Spatial control of arm movements. Exp Brain Res 42:223–227

Mussa-Ivaldi FA, Hogan N, Bizzi E (1985) Neural, mechanical, and geometric factors subserving arm posture in humans. J Neurosci 5(10):2732–2742

Özkaya N, Nordin M (1991) Fundamentals of biomechanics: equilibrium, motion, and deformation. Van Nostrand Reinhold, New York

Polit A, Bizzi E (1979) Characteristics of the motor programs underlying arm movements in monkeys. J Neurophysiol 42:183–194

Rack PMH, Westbury DR (1969) The effects of length and stimulus rate on tension in the isometric cat soleus muscle. J Physiol (Lond) 204:443–460

Sanger T (1992) Learning inverse dynamics by local exploration. Abstr Neural Networks for Computing Snowbird, Utah

Tsuji T, Ito K, Nagamachi M, Ikemoto T (1988) Impedance regulations in musculo-motor control system and the manipulation ability of the end-point. SICE 24(4):385–392 (in Japanese)

Uno Y, Kawato M, Suzuki R (1989) Formation and control of optimal trajectory in human multijoint arm movement: minimum-torque-change model. Biol Cybern 61:89–101

Wood JE, Meek SG, Jacobsen SC (1989a) Quantitation of human shoulder anatomy for prosthetic arm control. I. Surface modeling. J Biomech 22(3):273–292

Wood JE, Meek SG, Jacobsen SC (1989b) Quantitation of human shoulder anatomy for prosthetic arm control. II. Anatomy matrices. J Biomech 22(4):309–325